Q. J. R. Meteorol. Soc. (1997), **123**, pp. 1829–1840

Particle trajectories above sinusoidal terrain

By J. E. STOUT[1]* and G. S. JANOWITZ[2]
[1] *USDA–Agricultural Research Service, USA*
[2] *North Carolina State University, USA*

(Received 3 May 1996; revised 13 January 1997)

SUMMARY

As heavy particles fall towards windswept topography, their motion is governed partly by gravitational forces and partly by fluid forces resulting from the relative motion of the particles through the flow field. Topographically induced perturbations of the flow field distort particle paths and ultimately modify deposition patterns at the surface. Here, we calculate trajectories of particles falling toward a series of low-amplitude hills. Particle motion is obtained by simplifying the dynamical equations of particle motion to kinematic form and then applying perturbation techniques. This simplification is possible when the timescale of fluid motions is much longer than the characteristic response-time of the particles. It is shown that, under the right atmospheric conditions, alternating regions of convergent and divergent particle-paths will occur. An extension of the trajectory analysis yields expressions that predict the point of surface impact as functions of the initial release point. This leads to a method for predicting the point along the surface where deposition is either a maximum or a minimum.

KEYWORDS: Deposition Gravity waves Orography

1. INTRODUCTION

Stout *et al.* (1993) calculated trajectories for particles falling towards low-amplitude sinusoidal hills and it was shown that under the right atmospheric conditions, focusing of particle paths will occur. Particle motion was computed numerically by solving the Newtonian equations of motion for each particle. In the present paper, we show that similar results can be obtained analytically by first simplifying the equations of particle motion to kinematic form and then applying perturbation methods. We then extend the trajectory analysis to obtain expressions that predict the point of surface impact as functions of the point of initial release and knowledge of the flow structure. This leads to a method for predicting the point along the surface where deposition is a maximum or a minimum.

2. THEORY

We consider particles falling towards terrain with a surface which is described by a simple sinusoidal function with amplitude h, wavelength L, and wave number $k = 2\pi/L$

$$H(x) = h \sin(kx). \tag{1}$$

The magnitude of the maximum slope of terrain with sinusoidal surface is

$$\varepsilon \equiv \left| \frac{\mathrm{d}H}{\mathrm{d}x} \right|_{\max} = kh. \tag{2}$$

(*a*) *Particle motion*

The horizontal, lateral, and vertical coordinates are denoted (x, y, z) with unit vectors $(\mathbf{i}, \mathbf{j}, \mathbf{k})$. The coordinate system is oriented so that the gravitational vector acts parallel to the z-axis in the $-\mathbf{k}$ direction. The particle velocity vector is $\mathbf{V}_\mathrm{p} = (u_\mathrm{p}, v_\mathrm{p}, w_\mathrm{p})$, and the fluid velocity at the position of the particle is $\mathbf{V} = (u, v, w)$. The relative velocity vector is $\mathbf{V}_\mathrm{rel} = \mathbf{V} - \mathbf{V}_\mathrm{p}$ which is the fluid velocity as seen by an observer moving with the particle. The relative wind vector has components $\mathbf{V}_\mathrm{rel} = (u_\mathrm{rel}, v_\mathrm{rel}, w_\mathrm{rel})$.

* Corresponding author: US Department of Agriculture, Agricultural Research Service, Route 3, Block 215, Lubbock, Texas 79401, USA.

The drag of spherical particles has been studied extensively (see, for example, Zham (1926)). In its most general form, the drag-force vector may be expressed as

$$\mathbf{F}_{\mathrm{D}} = C_{\mathrm{D}} \frac{\pi D^2}{8} \rho V_{\mathrm{rel}} \mathbf{V}_{\mathrm{rel}}, \tag{3}$$

where C_{D} is the drag coefficient, D is the particle diameter, ρ is the fluid density, and V_{rel} is the magnitude of the resultant relative velocity vector $\mathbf{V}_{\mathrm{rel}}$. The gravitational force acting on a particle is

$$\mathbf{F}_{\mathrm{g}} = \frac{\pi D^3}{6} (\rho_{\mathrm{p}} - \rho) \mathbf{g}, \tag{4}$$

where ρ_{p} is the particle density and the gravitational vector $\mathbf{g} = -g\mathbf{k}$. Vectorially summing the fluid drag and gravitational forces acting on a particle and dividing by the particle mass gives the equation of particle motion as (Stout *et al.* 1995)

$$\frac{\mathrm{d}\mathbf{V}_{\mathrm{p}}}{\mathrm{d}t} = \frac{3}{4} \frac{\rho}{\rho_{\mathrm{p}}} \frac{C_{\mathrm{D}}}{D} V_{\mathrm{rel}} \mathbf{V}_{\mathrm{rel}} + \frac{\rho_{\mathrm{p}} - \rho}{\rho_{\mathrm{p}}} \mathbf{g}. \tag{5}$$

The first term on the right-hand side expresses the acceleration of the particle because of fluid drag, and the second term expresses the acceleration under gravity.

Time and velocity scales are introduced, and used to give non-dimensional variable forms

$$\widehat{t} = \frac{t}{T}; \quad \widehat{\mathbf{V}}_{\mathrm{p}} = \frac{\mathbf{V}_{\mathrm{p}}}{W_{\mathrm{T}}}; \quad \widehat{\mathbf{V}}_{\mathrm{rel}} = \frac{\mathbf{V}_{\mathrm{rel}}}{W_{\mathrm{T}}}, \tag{6}$$

where $T \equiv (mW_{\mathrm{T}})^{-1}$ is the timescale of fluid motions as 'seen' by a particle falling vertically at terminal velocity W_{T} through a fluid with vertical wave-number

$$m \equiv |\ell^2 - k^2|^{1/2}. \tag{7}$$

Here, the Scorer parameter is denoted by ℓ and for the case of no mean shear $\ell = N/U$, where N is the Brunt–Väisälä frequency and U is the basic wind speed. The terminal velocity is

$$W_{\mathrm{T}} \equiv \left(\frac{4}{3} \frac{D}{C_{\mathrm{D_T}}} g \frac{\rho_{\mathrm{p}} - \rho}{\rho} \right)^{1/2}, \tag{8}$$

where $C_{\mathrm{D_T}}$ is the drag coefficient at terminal velocity. Combining Eqs. (5), (6), and (8) yields the non-dimensional form of the equation of motion

$$\frac{\mathrm{d}\widehat{\mathbf{V}}_{\mathrm{p}}}{\mathrm{d}\widehat{t}} = \alpha \left(\frac{C_{\mathrm{D}}}{C_{\mathrm{D_T}}} \widehat{V}_{\mathrm{rel}} \widehat{\mathbf{V}}_{\mathrm{rel}} - \mathbf{k} \right). \tag{9}$$

The dimensionless parameter α is

$$\alpha \equiv \frac{g(1 - \rho/\rho_{\mathrm{p}})}{mW_{\mathrm{T}}^2} = \frac{T}{\tau_{\mathrm{p}}}, \tag{10}$$

and may be interpreted as the ratio of the timescale T of the fluid motions (as seen by a falling particle) to the particle response time τ_{p}, defined as

$$\tau_{\mathrm{p}} \equiv \frac{W_{\mathrm{T}}}{g(1 - \rho/\rho_{\mathrm{p}})}. \tag{11}$$

This timescale has been shown to be appropriate for particles undergoing linear or nonlinear drag (Stout *et al.* 1995). For Stokes flow (linear drag) τ_p reduces to the standard form $\rho_p D/18\mu$, where μ is the fluid viscosity (Fuchs 1964).

An interesting limiting case is obtained when the timescale of fluid motions is much longer than the response time of the particle, i.e. $T \gg \tau_p$ or α is very large. This condition is normally satisfied when small particles fall towards large-scale topographic flows; each particle is then able to adjust immediately to follow changes in fluid motions. Dividing the equations of motion by α, and taking the limit as α tends to infinity, we find that the only relative motion is in the direction of the gravitational body force. Thus, as α tends to infinity, then $\hat{u}_{rel} \to 0$, $\hat{v}_{rel} \to 0$, $\hat{w}_{rel} \to 1$ and $C_D/C_{D_T} \to 1$. In this case, the equation of particle motion (Eq. (9)) reduces to kinematic form as

$$\hat{\mathbf{V}}_p = \hat{\mathbf{V}} - \mathbf{k}. \tag{12}$$

In other words, particle motion follows the fluid motion except for a constant drift velocity in the direction of the gravitational body force, equal in magnitude to the terminal velocity.

The particle velocity can be expressed as the rate of change of the particle position-vector. For two-dimensional motion, the dimensionless position-vector $\hat{\mathbf{R}}$ is

$$\hat{\mathbf{R}} = kX\mathbf{i} + mZ\mathbf{k} = \hat{X}\mathbf{i} + \hat{Z}\mathbf{k}, \tag{13}$$

and the dimensionless particle-velocity-vector is

$$\hat{\mathbf{V}}_p = \frac{d\hat{\mathbf{R}}}{d\hat{t}} = \frac{m}{k}\frac{d\hat{X}}{d\hat{t}}\mathbf{i} + \frac{d\hat{Z}}{d\hat{t}}\mathbf{k}. \tag{14}$$

We consider a two-dimensional flow with a fluid-velocity-vector

$$\hat{\mathbf{V}} = \hat{u}\mathbf{i} + \hat{w}\mathbf{k}. \tag{15}$$

Combining Eqs. (12), (14), and (15) and separating components yields the following expressions for particle motion

$$\frac{d\hat{X}}{d\hat{t}} = \frac{k}{m}\hat{u}(\hat{X}, \hat{Z}), \tag{16}$$

$$\frac{d\hat{Z}}{d\hat{t}} = \hat{w}(\hat{X}, \hat{Z}) - 1. \tag{17}$$

Thus, as the particle falls through a moving fluid, it is assumed to adjust immediately to match the horizontal fluid-flow and the vertical velocity of each particle is assumed to adjust immediately to fall at the particle's terminal velocity relative to the surrounding fluid.

(*b*) *Fluid motions*

Solutions for two-dimensional flow over sinusoidal terrain were obtained from linear theory by Queney (1948) and have been summarized by Smith (1979). Linear theory is based upon the small-amplitude assumption which requires that $kh \ll 1$ where $\ell^2/k^2 < 1$ (weak stratification) and $\ell h \ll 1$ where $\ell^2/k^2 > 1$ (strong stratification).

For strong flow in a weakly stratified atmosphere with narrow hills ($\ell^2/k^2 < 1$), the flow field above sinusoidal terrain consists of evanescent waves. The horizontal and vertical components of the fluid velocity are

$$\hat{u}(\hat{X}, \hat{Z}) = \frac{U}{W_T} + \varepsilon\frac{m}{k}\frac{U}{W_T}\sin(\hat{X})\,e^{-\hat{Z}}, \tag{18}$$

$$\widehat{w}(\widehat{X}, \widehat{Z}) = \varepsilon \frac{U}{W_T} \cos(\widehat{X})\, e^{-\widehat{Z}}. \tag{19}$$

Here, the flow field is expressed as a function of the particle position $(\widehat{X}, \widehat{Z})$.

For weak flow in strong stratification over a series of wide hills $(\ell^2/k^2 > 1)$, the flow field above sinusoidal terrain consists of a series of vertically propagating waves. The flow field may be written as

$$\widehat{u}(\widehat{X}, \widehat{Z}) = \frac{U}{W_T} - \varepsilon \frac{m}{k} \frac{U}{W_T} \cos(\widehat{X} + \widehat{Z}), \tag{20}$$

$$\widehat{w}(\widehat{X}, \widehat{Z}) = \varepsilon \frac{U}{W_T} \cos(\widehat{X} + \widehat{Z}). \tag{21}$$

3. Vertically propagating waves $(\ell^2/k^2 > 1)$

(a) *Particle trajectories (vertically propagating waves)*

In this subsection, we derive expressions for the motion of particles falling through vertically propagating waves. Particle position is expressed as an asymptotic expansion assuming $\varepsilon \ll 1$,

$$\widehat{X} = \widehat{X}_0 + \varepsilon \widehat{X}_1 + \varepsilon^2 \widehat{X}_2 + \cdots \tag{22}$$

$$\widehat{Z} = \widehat{Z}_0 + \varepsilon \widehat{Z}_1 + \varepsilon^2 \widehat{Z}_2 + \cdots. \tag{23}$$

The fluid-velocity equations for vertically propagating waves (Eqs. (20) and (21)) are rewritten using the asymptotic expansions for $\widehat{X}$ and $\widehat{Z}$ (Eqs. (22) and (23)) which yield the following expanded forms

$$\widehat{u}(\widehat{X}, \widehat{Z}) = \frac{U}{W_T} - \varepsilon \frac{m}{k} \frac{U}{W_T} \cos(\widehat{X}_0 + \widehat{Z}_0) + O(\varepsilon^2), \tag{24}$$

$$\widehat{w}(\widehat{X}, \widehat{Z}) = \varepsilon \frac{U}{W_T} \cos(\widehat{X}_0 + \widehat{Z}_0) + O(\varepsilon^2). \tag{25}$$

Insertion of Eqs. (24) and (25) into Eqs. (16) and (17) and using Eqs. (22) and (23) yields the expanded kinematic equations for particles falling through vertically propagating waves as

$$\frac{d\widehat{X}_0}{d\widehat{t}} + \varepsilon \frac{d\widehat{X}_1}{d\widehat{t}} + O(\varepsilon^2) = \phi - \varepsilon \frac{U}{W_T} \cos(\widehat{X}_0 + \widehat{Z}_0) + O(\varepsilon^2), \tag{26}$$

$$\frac{d\widehat{Z}_0}{d\widehat{t}} + \varepsilon \frac{d\widehat{Z}_1}{d\widehat{t}} + O(\varepsilon^2) = -1 + \varepsilon \frac{U}{W_T} \cos(\widehat{X}_0 + \widehat{Z}_0) + O(\varepsilon^2), \tag{27}$$

where

$$\phi \equiv \frac{k}{m} \frac{U}{W_T}. \tag{28}$$

The guiding principle of perturbation theory is that since the expansions must hold for arbitrary values of the perturbation quantity ε, terms of like order in ε must separately satisfy each equality (Van Dyke 1964). Thus, we can separate terms of like order. Integration of the lowest-order terms yields the zeroth approximation which may be written as

$$\widehat{X}_0(t) = \widehat{X}_i + \phi \widehat{t}, \tag{29}$$

$$\widehat{Z}_0(t) = \widehat{Z}_i - \widehat{t}, \tag{30}$$

where the initial release point is denoted by $(\widehat{X}_i, \widehat{Z}_i)$. This straight-line trajectory is equivalent to the solution for particles falling within a layer of uniform flow above flat terrain. Integration of the first-order equations yields the first-order corrections as

$$\widehat{X}_1(\widehat{t}) = -\frac{m}{k}\frac{\phi}{\phi - 1}\{\sin(\widehat{X}_i + \widehat{Z}_i + (\phi - 1)\widehat{t}) - \sin(\widehat{X}_i + \widehat{Z}_i)\}, \tag{31}$$

$$\widehat{Z}_1(\widehat{t}) = \frac{m}{k}\frac{\phi}{\phi - 1}\{\sin(\widehat{X}_i + \widehat{Z}_i + (\phi - 1)\widehat{t}) - \sin(\widehat{X}_i + \widehat{Z}_i)\}. \tag{32}$$

Ignoring second-order and higher terms, the full solution for the vertically propagating wave-regime is obtained by combining the zeroth approximations and the first-order corrections as follows

$$\widehat{X}(\widehat{t}) = \widehat{X}_i + \phi\widehat{t} - \frac{mh\phi}{\phi - 1}\{\sin(\widehat{X}_i + \widehat{Z}_i + (\phi - 1)\widehat{t}) - \sin(\widehat{X}_i + \widehat{Z}_i)\}, \tag{33}$$

$$\widehat{Z}(\widehat{t}) = \widehat{Z}_i - \widehat{t} + \frac{mh\phi}{\phi - 1}\{\sin(\widehat{X}_i + \widehat{Z}_i + (\phi - 1)\widehat{t}) - \sin(\widehat{X}_i + \widehat{Z}_i)\}. \tag{34}$$

This solution consists of a straight-line trajectory, defined by the first two terms of each equation, and a perturbation term that reflects the effects of topography. A unique trajectory is defined by four dimensionless parameters $\widehat{X}_i$, $\widehat{Z}_i$, ϕ and mh.

A comparison of trajectories predicted by the analytical expressions derived here with numerical predictions by Stout *et al.* (1993) is shown in Fig. 1. Here, $h = 200$ m, $L = 4000$ m, $U = 10$ m s^{-1}, $W_T = 4$ m s^{-1}, and $N = 0.02$ s^{-1} or in non-dimensional form $mh = 0.25$, $\phi = 3.17$, $\widehat{Z}_i = 2.5$, and $\widehat{X}_i$ varies from 0 to 4π. A comparison reveals that the overall trajectory-pattern appears to be well represented by both the numerical solution of the full particle-dynamics equations and by the analytical expressions derived here using the immediate adjustment approximation. However, some small differences may be the result of different initial conditions. Stout *et al.* (1993) allowed all particles to be released with no initial vertical velocity, whereas, in the present paper, the immediate adjustment approximation determines the release conditions. For vertically propagating waves, fluid perturbations are present at the release height, so that under the immediate adjustment approximation the particle velocity at release depends on the initial release-point within the fluid.

The magnitude of mh affects the magnitude of the perturbation term, but mh is restricted to values much less than unity as a result of the small amplitude assumption invoked in linear theory. Perhaps the most interesting of these four terms is ϕ, which expresses the relative slope of the constant-phase lines of the fluid flow to the natural fall angle of the particle motion. A series of trajectories is plotted in Fig. 2, in which the value of ϕ is systematically varied. Note that when $\phi < 1$, which corresponds to a fall angle that is larger than the angle of the constant-phase lines, the particle paths are fairly straight, and the trajectory patterns are not considerably different from those above flat terrain. Where $\phi > 1$, which corresponds to a fall angle that is shallower than the angle of the constant-phase lines, we find a focusing of particle paths which increases with increasing ϕ.

When $\phi = 1$, which corresponds to a fall angle exactly equal to the slope of the constant-phase lines, we obtain the indeterminate form 0/0 for the perturbation terms. Using L'Hôpital's rule, we find that in the limit as the value of ϕ tends to one, the perturbation

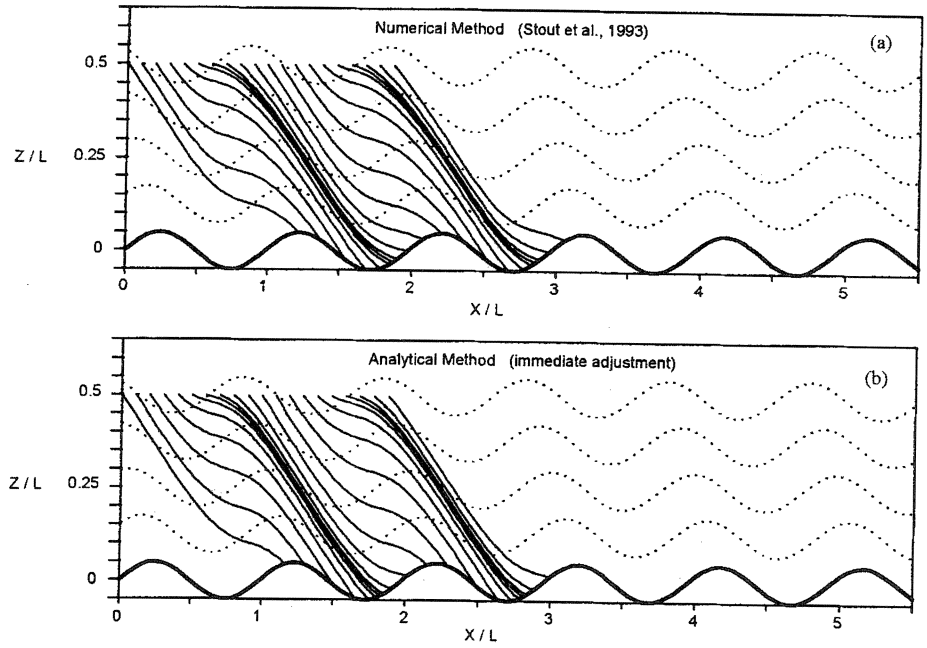

Figure 1. Comparison of calculated trajectory patterns for particles falling through vertically propagating waves with $mh = 0.25$ and $\phi = 3.17$.

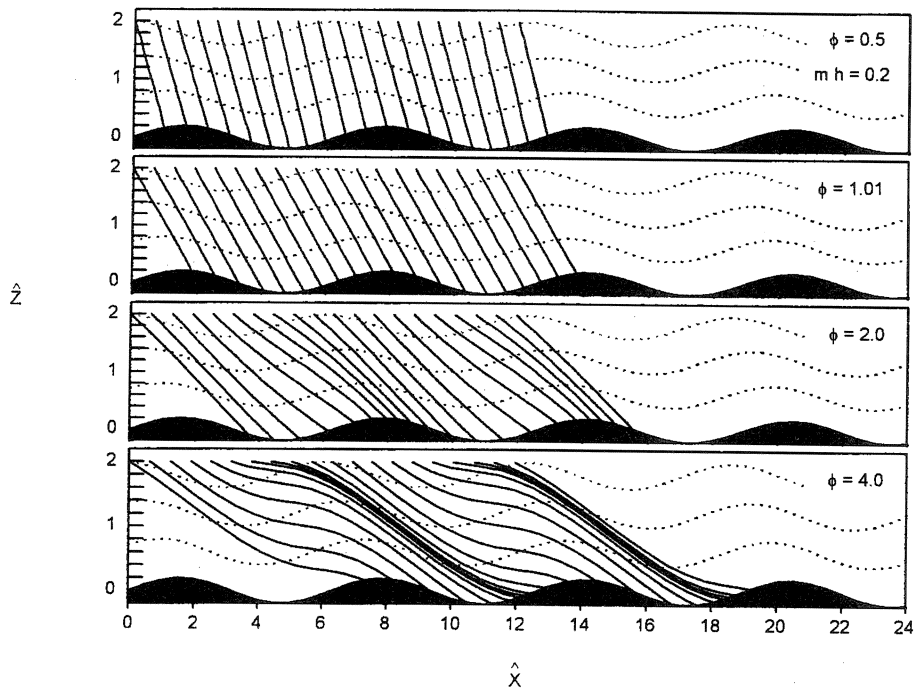

Figure 2. Series of trajectories plotted for particles falling through vertically propagating waves.

terms are well behaved and the trajectories are straight lines. In Fig. 2, we avoid this problem by choosing a value of $\phi = 1.01$, a value that is very close to, but not equal to, unity.

(*b*) *Impact location (vertically propagating waves)*

In the previous subsection, expressions were derived for the trajectories of particles falling through vertically propagating waves. Extending this analysis to predict the point of surface impact is not difficult. In a steady flow, a one-to-one correspondence exists between the initial release point $(\hat{X}_i, \hat{Z}_i)$ and the surface impact location $(\hat{X}_*, \hat{Z}_*)$.

Recall that the trajectory of a particle falling through vertically propagating waves may be expressed as

$$\hat{X}(\hat{t}) = \hat{X}_i + \phi\hat{t} - \varepsilon\frac{m}{k}F(\hat{X}_i, \hat{Z}_i, \hat{t}), \tag{35}$$

$$\hat{Z}(\hat{t}) = \hat{Z}_i - \hat{t} + \varepsilon\frac{m}{k}F(\hat{X}_i, \hat{Z}_i, \hat{t}), \tag{36}$$

where the function F is

$$F(\hat{X}_i, \hat{Z}_i, \hat{t}) \equiv \frac{\phi}{\phi - 1}\{\sin(\hat{X}_i + \hat{Z}_i + (\phi - 1)\hat{t}) - \sin(\hat{X}_i + \hat{Z}_i)\}. \tag{37}$$

Time is expressed as an asymptotic expansion as

$$\hat{t} = \hat{t}_0 + \varepsilon\hat{t}_1 + \cdots. \tag{38}$$

We denote the time and position at the moment of surface impact by a subscripted asterisk. The horizontal and vertical particle positions at impact are

$$\hat{X}_*(\hat{t}_*) = \hat{X}_{*0} + \varepsilon\hat{X}_{*1} = \hat{X}_i + \phi\hat{t}_{*0} + \phi\varepsilon\hat{t}_{*1} - \varepsilon\frac{m}{k}F(\hat{X}_i, \hat{Z}_i, \hat{t}_*), \tag{39}$$

$$\hat{Z}_*(\hat{t}_*) = \hat{Z}_{*0} + \varepsilon\hat{Z}_{*1} = \hat{Z}_i - \hat{t}_{*0} - \varepsilon\hat{t}_{*1} + \varepsilon\frac{m}{k}F(\hat{X}_i, \hat{Z}_i, \hat{t}_*) = \varepsilon\frac{m}{k}\sin(\hat{X}_{*0}). \tag{40}$$

To lowest order we find that

$$\hat{t}_{*0} = \hat{Z}_i, \tag{41}$$

and

$$\hat{X}_{*0} = \hat{X}_i + \phi\hat{Z}_i. \tag{42}$$

Thus, we can rewrite the function F as

$$F(\hat{X}_i, \hat{Z}_i, t_{*0}) = \frac{\phi}{\phi - 1}\{\sin(\hat{X}_i + \phi\hat{Z}_i) - \sin(\hat{X}_i + \hat{Z}_i)\}. \tag{43}$$

The first-order correction for time is obtained from Eq. (40) as

$$\hat{t}_{*1} = \frac{m}{k}\frac{1}{\phi - 1}\{\sin(\hat{X}_i + \phi\hat{Z}_i) - \phi\sin(\hat{X}_i + \hat{Z}_i)\}. \tag{44}$$

Inserting Eq. (44) into Eq. (39) yields the final expression for the horizontal position of surface impact as a function of the initial release point

$$\hat{X}_*(\hat{X}_i, \hat{Z}_i) = \hat{X}_i + \phi\hat{Z}_i - mh\phi\sin(\hat{X}_i + \hat{Z}_i). \tag{45}$$

Note that the horizontal impact location generally grows linearly with $\hat{Z}_i$, as it would above a simpler flat surface, but, here, an additional perturbation-term reflects the effect of topography. The perturbation term becomes less important as the steepness of the topography kh is reduced and as the basic angle of fall W_T/U becomes larger (particles fall more vertically).

The impact height is

$$\hat{Z}_*(\hat{X}_*) = mh \sin(\hat{X}_*). \tag{46}$$

Now that we have obtained a relationship between the release point and the final destination of the particles, we can answer an important question about trajectory spacing. Along the surface, the horizontal spacing of individual trajectories is inversely proportional to the surface deposition of particles. Given an initial spacing $\partial \hat{X}_i$, the change of surface spacing of trajectories $\partial \hat{X}_*$ is

$$\frac{\partial \hat{X}_*}{\partial \hat{X}_i} = 1 - mh\phi \cos(\hat{X}_i + \hat{Z}_i), \tag{47}$$

which has a minimum when $\hat{X}_i + \hat{Z}_i = 2\pi n$, where $n = 0, 1, 2, \ldots$. Thus, maximum deposition (corresponding to minimum trajectory spacing) occurs where

$$\hat{X}_{*\max} = 2\pi n + (\phi - 1)\hat{Z}_i. \tag{48}$$

For $\phi = 4$ and $\hat{Z}_i = 2$, we find that $\hat{X}_{*\max} = 12.28$ and 18.57 for $n = 1$ and 2 respectively. From Fig. 2 we find that this agrees closely with the point along the surface with the closest spacing of particle trajectories. The maximum trajectory spacing is found when $\hat{X}_i + \hat{Z}_i = 2\pi(n + 1/2)$, where $n = 0, 1, 2 \ldots$. Thus, minimum deposition occurs where

$$\hat{X}_{*\min} = 2\pi(n + 1/2) + (\phi - 1)\hat{Z}_i. \tag{49}$$

For $\phi = 4$ and $\hat{Z}_i = 2$, we find that $\hat{X}_{*\min} = 9.14$ and 15.42 for $n = 0$ and 1, respectively. Again we find that this agrees closely with Fig. 2.

4. Evanescent waves ($\ell^2/k^2 < 1$)

(a) *Particle trajectories (evanescent waves)*

In this subsection, we derive analytical expressions for the motion of particles falling through evanescent waves. Using Eqs. (22) and (23), we expand the fluid-velocity equations for evanescent waves (Eqs. (18) and (19)) as

$$\hat{u}(\hat{X}, \hat{Z}) = \frac{U}{W_T} + \varepsilon \frac{m}{k}\frac{U}{W_T} \sin(\hat{X}_0)\, e^{-\hat{Z}_0} + O(\varepsilon^2), \tag{50}$$

$$\hat{w}(\hat{X}, \hat{Z}) = \varepsilon \frac{U}{W_T} \cos(\hat{X}_0)\, e^{-\hat{Z}_0} + O(\varepsilon^2). \tag{51}$$

Inserting Eqs. (50) and (51) into Eqs. (16) and (17) and using the expansions Eqs. (22) and (23) yields the expanded kinematic equations for particles falling through evanescent waves as

$$\frac{d\hat{X}_0}{d\hat{t}} + \varepsilon \frac{d\hat{X}_1}{d\hat{t}} + O(\varepsilon^2) = \phi + \varepsilon \frac{U}{W_T} \sin(\hat{X}_0)\, e^{-\hat{Z}_0} + O(\varepsilon^2), \tag{52}$$

$$\frac{\mathrm{d}\hat{Z}_0}{\mathrm{d}\hat{t}} + \varepsilon\frac{\mathrm{d}\hat{Z}_1}{\mathrm{d}\hat{t}} + \mathrm{O}(\varepsilon^2) = -1 + \varepsilon\frac{U}{W_\mathrm{T}}\cos(\hat{X}_0)\,\mathrm{e}^{-\hat{Z}_0} + \mathrm{O}(\varepsilon^2). \tag{53}$$

As with the previous case, we obtain a straight-line trajectory as the zeroth approximation (see Eqs. (29) and (30)). Integration of the first-order equations yields the first-order corrections as

$$\hat{X}_1(\hat{t}) = \frac{-m}{k}\frac{\phi}{1+\phi^2}[\mathrm{e}^{\hat{t}-\hat{Z}_\mathrm{i}}\{\phi\cos(\hat{X}_\mathrm{i}+\phi\hat{t}) - \sin(\hat{X}_\mathrm{i}+\phi\hat{t})\}$$

$$-\mathrm{e}^{-\hat{Z}_\mathrm{i}}\{\phi\cos(\hat{X}_\mathrm{i}) - \sin(\hat{X}_\mathrm{i})\}], \tag{54}$$

$$\hat{Z}_1(\hat{t}) = \frac{m}{k}\frac{\phi}{1+\phi^2}[\mathrm{e}^{\hat{t}-\hat{Z}_\mathrm{i}}\{\cos(\hat{X}_\mathrm{i}+\phi\hat{t}) + \phi\sin(\hat{X}_\mathrm{i}+\phi\hat{t})\}$$

$$-\mathrm{e}^{-\hat{Z}_\mathrm{i}}\{\cos(\hat{X}_\mathrm{i}) + \phi\sin(\hat{X}_\mathrm{i})\}]. \tag{55}$$

Ignoring second-order and higher terms, the full solution is obtained by combining the zeroth approximations and the first-order corrections as follows

$$\hat{X}(\hat{t}) = \hat{X}_\mathrm{i} + \phi\hat{t} - \frac{mh\phi}{1+\phi^2}[\mathrm{e}^{\hat{t}-\hat{Z}_\mathrm{i}}\{\phi\cos(\hat{X}_\mathrm{i}+\phi\hat{t}) - \sin(\hat{X}_\mathrm{i}+\phi\hat{t})\}$$

$$-\mathrm{e}^{-\hat{Z}_\mathrm{i}}\{\phi\cos(\hat{X}_\mathrm{i}) - \sin(\hat{X}_\mathrm{i})\}], \tag{56}$$

$$\hat{Z}(\hat{t}) = \hat{Z}_\mathrm{i} - \hat{t} + \frac{mh\phi}{1+\phi^2}[\mathrm{e}^{\hat{t}-\hat{Z}_\mathrm{i}}\{\cos(\hat{X}_\mathrm{i}+\phi\hat{t}) + \phi\sin(\hat{X}_\mathrm{i}+\phi\hat{t})\}$$

$$-\mathrm{e}^{-\hat{Z}_\mathrm{i}}\{\cos(\hat{X}_\mathrm{i}) + \phi\sin(\hat{X}_\mathrm{i})\}]. \tag{57}$$

As with the previous case, we find that a unique trajectory is defined by four dimensionless parameters $\hat{X}_\mathrm{i}$, $\hat{Z}_\mathrm{i}$, ϕ and mh. Trajectories of particles falling through evanescent waves predicted by the analytical expressions derived here, along with numerical predictions from Stout *et al.* (1993), are shown in Fig. 3. In this case, $h = 200$ m, $L = 4000$ m, $U = 10$ m s^{-1}, $W_\mathrm{T} = 4$ m s^{-1}, and $N = 0.01$ s^{-1} or in non-dimensional terms $mh = 0.24$, $\phi = 3.24$, and $\hat{Z}_\mathrm{i} = 2.4$. The derived analytical expressions describe the general trajectory pattern quite well. Panels (a) and (b) in Fig. 3 agree more closely than the corresponding panels in Fig. 1. Most probably, this is because the fluid perturbations at the given release height are negligible for evanescent waves and, therefore, the initial conditions are nearly identical.

A number of trajectories are plotted in Fig. 4, in which the value of ϕ is doubled. Here, there is no problem when $\phi = 1$ since the denominator contains the term $1 + \phi^2$. When $\phi < 1$, the particle paths are fairly straight and the trajectory patterns are not considerably different from those above flat terrain. Where $\phi > 1$, we find more substantial perturbations in the particle paths, but we still do not find strong focusing with increasing ϕ. This reveals that evanescent waves do not produce such strong focusing as do vertically propagating waves.

(*b*) *Impact location (evanescent waves)*

Recall that the particle trajectory for evanescent waves may be expressed as

$$\hat{X}(t) = \hat{X}_\mathrm{i} + \phi\hat{t} - \varepsilon\frac{m}{k}F_x(\hat{X}_\mathrm{i}, \hat{Z}_\mathrm{i}, \hat{t}), \tag{58}$$

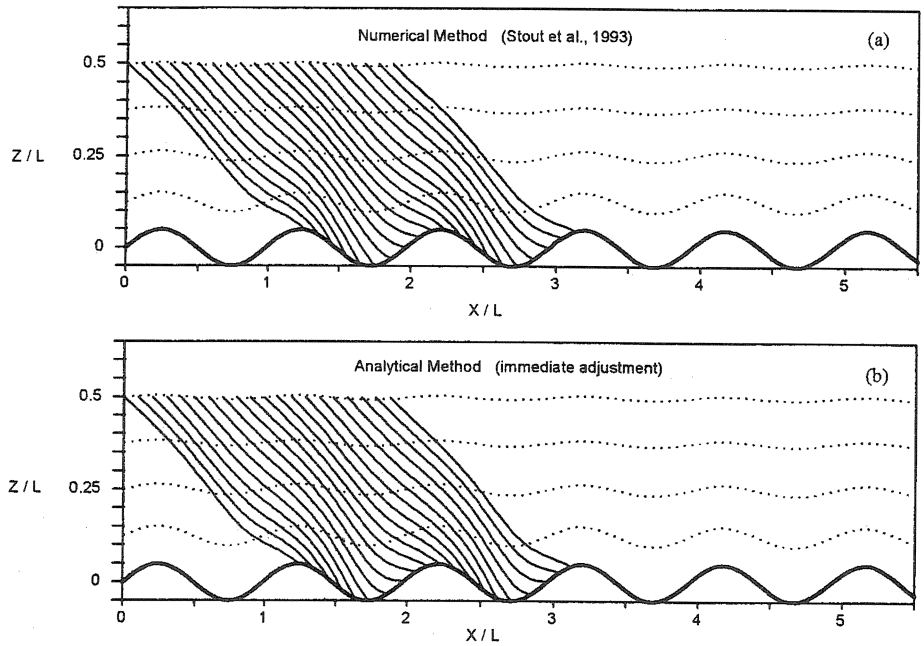

Figure 3. Comparison of calculated trajectory patterns for particles falling through evanescent waves with $mh = 0.24$ and $\phi = 3.24$.

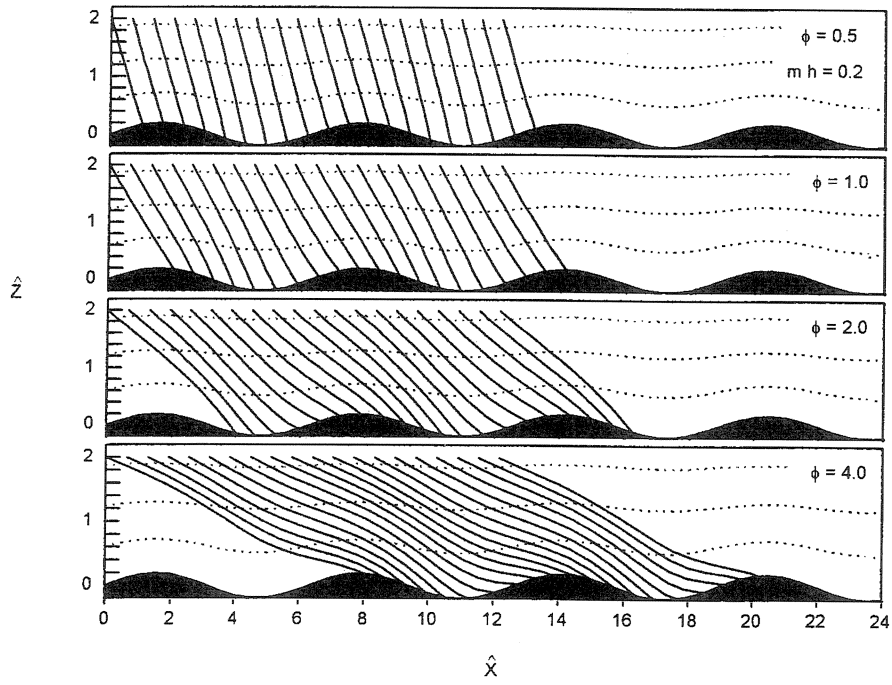

Figure 4. Series of trajectories plotted for particles falling through evanescent waves.

$$\widehat{Z}(\widehat{t}) = \widehat{Z}_{\mathrm{i}} - \widehat{t} + \varepsilon \frac{m}{k} F_z(\widehat{X}_{\mathrm{i}}, \widehat{Z}_{\mathrm{i}}, \widehat{t}). \tag{59}$$

For evanescent waves, F_x and F_z are

$$F_x = \frac{\phi}{1+\phi^2}[\mathrm{e}^{\hat{t}-\hat{Z}_{\mathrm{i}}}\{\phi\cos(\widehat{X}_{\mathrm{i}} + \phi\widehat{t}) - \sin(\widehat{X}_{\mathrm{i}} + \phi\widehat{t})\}$$

$$-\mathrm{e}^{-\hat{Z}_{\mathrm{i}}}\{\phi\cos(\widehat{X}_{\mathrm{i}}) - \sin(\widehat{X}_{\mathrm{i}})\}], \tag{60}$$

$$F_z = \frac{\phi}{1+\phi^2}[\mathrm{e}^{\hat{t}-\hat{Z}_{\mathrm{i}}}\{\cos(\widehat{X}_{\mathrm{i}} + \phi\widehat{t}) + \phi\sin(\widehat{X}_{\mathrm{i}} + \phi\widehat{t})\}$$

$$-\mathrm{e}^{-\hat{Z}_{\mathrm{i}}}\{\cos(\widehat{X}_{\mathrm{i}}) + \phi\sin(\widehat{X}_{\mathrm{i}})\}]. \tag{61}$$

Substituting the asymptotic expansion for time (Eq. (38)) yields the horizontal and vertical particle-position at the moment of surface impact as

$$\widehat{X}_* = \widehat{X}_{*0} + \varepsilon\widehat{X}_{*1} = \widehat{X}_{\mathrm{i}} + \phi\widehat{t}_{*0} + \varepsilon\phi\widehat{t}_{*1} - \varepsilon\frac{m}{k}F_{*x}, \tag{62}$$

$$\widehat{Z}_* = \widehat{Z}_{*0} + \varepsilon\widehat{Z}_{*1} = \widehat{Z}_{\mathrm{i}} - \widehat{t}_{*0} - \varepsilon\widehat{t}_{*1} + \varepsilon\frac{m}{k}F_{*z} = \varepsilon\frac{m}{k}\sin(\widehat{X}_{*0}). \tag{63}$$

To lowest order we find that

$$\widehat{t}_{*0} = \widehat{Z}_{\mathrm{i}}, \tag{64}$$

$$\widehat{X}_{*0} = \widehat{X}_{\mathrm{i}} + \phi\widehat{Z}_{\mathrm{i}}. \tag{65}$$

So we can rewrite the functions F_{*x} and F_{*z} at the surface as

$$F_{*x} = \frac{\phi}{1+\phi^2}[\phi\cos(\widehat{X}_{\mathrm{i}} + \phi\widehat{Z}_{\mathrm{i}}) - \sin(\widehat{X}_{\mathrm{i}} + \phi\widehat{Z}_{\mathrm{i}}) - \mathrm{e}^{-\hat{Z}_{\mathrm{i}}}\{\phi\cos(\widehat{X}_{\mathrm{i}}) - \sin(\widehat{X}_{\mathrm{i}})\}], \tag{66}$$

$$F_{*z} = \frac{\phi}{1+\phi^2}[\cos(\widehat{X}_{\mathrm{i}} + \phi\widehat{Z}_{\mathrm{i}}) + \phi\sin(\widehat{X}_{\mathrm{i}} + \phi\widehat{Z}_{\mathrm{i}}) - \mathrm{e}^{-\hat{Z}_{\mathrm{i}}}\{\cos(\widehat{X}_{\mathrm{i}}) + \phi\sin(\widehat{X}_{\mathrm{i}})\}]. \tag{67}$$

From Eq. (63), the first-order correction for time is

$$\widehat{t}_{*1} = \frac{m}{k}\{F_{*z} - \sin(\widehat{X}_{\mathrm{i}} + \phi\widehat{Z}_{\mathrm{i}})\}. \tag{68}$$

Substituting this expression into Eq. (62) yields the horizontal impact location for particles falling through evanescent waves as

$$\widehat{X}_*(\widehat{X}_{\mathrm{i}}, \widehat{Z}_{\mathrm{i}}) = \widehat{X}_{\mathrm{i}} + \phi\widehat{Z}_{\mathrm{i}} - mh\phi\,\mathrm{e}^{-\hat{Z}_{\mathrm{i}}}\sin(\widehat{X}_{\mathrm{i}}). \tag{69}$$

The change of trajectory spacing is

$$\frac{\partial\widehat{X}_*}{\partial\widehat{X}_{\mathrm{i}}} = 1 - mh\phi\,\mathrm{e}^{-\hat{Z}_{\mathrm{i}}}\cos(\widehat{X}_{\mathrm{i}}), \tag{70}$$

which has a minimum when $\widehat{X}_{\mathrm{i}} = 2\pi n$, where $n = 0, 1, 2 \ldots$. Thus, maximum deposition (corresponding to minimum trajectory-spacing) occurs where

$$\widehat{X}_{*\max} = 2\pi n + \phi\widehat{Z}_{\mathrm{i}}. \tag{71}$$

For $\phi = 4$ and $\widehat{Z}_i = 2$, we find that $\widehat{X}_{*\max} = 8.0$, 14.28, and 20.57 for $n = 0$, 1, and 2 respectively. Thus, the top of each hill will receive the largest deposition for the conditions specified.

The maximum trajectory-spacing is found when $\widehat{X}_i = 2\pi(n + 1/2)$, where $n = 0$, 1, 2 . . . . Thus, minimum deposition occurs where

$$\widehat{X}_{*\min} = 2\pi(n + 1/2) + \phi\widehat{Z}_i. \tag{72}$$

For $\phi = 4$ and $\widehat{Z}_i = 2$, we find that $\widehat{X}_{*\min} = 11.14$ and 17.42 for $n = 0$ and 1 respectively. Thus, the troughs would receive the least deposition for the conditions specified.

5. Summary

Analytical expressions are obtained for trajectories of particles falling through the spatially varying flow-field above sinusoidal terrain. We consider strong stratification with vertically propagating waves and weak stratification with evanescent waves. For such large-scale flows, where the fluid timescale is often two orders of magnitude longer than the particle response-time, we find that the immediate adjustment approximation is valid and can be used to simplify the equations of motion to kinematic form. Using perturbation methods, the kinematic equations are solved analytically to yield expressions for particle trajectories. Trajectories in the two wave-types are similar in that they contain a linear term to lowest order, but our results show that they are fundamentally different in the first-order correction term.

Expressions were derived that link the release height to the location of the final surface impact and a method was developed for predicting the point along the surface where maximum and minimum deposition occur.

Acknowledgements

We acknowledge the careful review of this manuscript by W. H. Snyder, NOAA, and Dr. S. P. Arya, North Carolina State University. This research has been supported by the U.S. Environmental Protection Agency under Cooperative Agreement CR 817931 with North Carolina State University. The contents of this paper do not necessarily reflect the views and policies of the Agency.

References

Fuchs, N. A. 1964 *The Mechanics of Aerosols.* Pergamon Press

Queney, P 1948 The problem of air flow over mountains: A summary of theoretical studies. *Bull. Am. Meteorol. Soc.*, **29,** 16–25

Smith, R. B. 1979 The influence of mountains on the atmosphere. Pp. 87–230 in *Advances in Geophysics*, **21,** Academic Press

Stout, J. E., Lin, Y.-L. and Arya, S. P. S. 1993 A theoretical investigation of the effects of sinusoidal topography on particle deposition. *J. Atmos. Sci.*, **50,** 2533–2541

Stout, J. E., Arya, S. P. and Genikhovich, E. L. 1995 The effect of nonlinear drag on the motion and settling velocity of heavy particles. *J. Atmos. Sci.*, **52,** 3836–3848

Van Dyke, M. 1964 *Perturbation Methods in Fluid Mechanics.* Academic Press

Zahm, A. F. 1926 Flow and drag formulas for simple quadrics. *NACA Tech. Rept.* No. 253